Study of Low-Aspect Ratio Swept and Oblique Wings

Edward J. Hopkins* and Alan D. Levin†
NASA Ames Research Center, Moffett Field, Calif.

Experimental forces and moments for two wing-body combinations having a) a swept wing and b) an oblique wing are compared. At all Mach numbers, the oblique wing (at its optimum sweep angle) had higher maximum lift-to-drag ratios than the fixed, swept wing. At high angles of attack, the direction of the pitching or rolling tendencies of the oblique wing was a function of the spanwise distribution of wing bend or washout for the two bends being investigated. At low angles of attack, linear theory gave satisfactory predictions of the subsonic lift-curve slope, the aerodynamic-center travel with Mach number, and the maximum lift-to-drag ratio.

Nomenclature

b	= wing span, 71.12 cm (28.00 in.)
c	= wing chord
$\bar{c}$	= wing mean aerodynamic chord, 20.88 cm (8.22 in.)
C_D	= drag coefficient, drag/qS
C_l	= rolling-moment coefficient about body axes, rolling-moment/qSb
C_L	= lift coefficient, lift/qS
C_{L_α}	= lift-curve slope at $\alpha=0$, per degree, $dC_L/d\alpha$
C_m	= pitching-moment coefficient, pitching-moment/$qS\bar{c}$
C_n	= yawing-moment coefficient about the body axes, yawing moment/qSb
$d(C_D)/d(\Delta C_L)^2$	= factor of drag due to lift, $K=d(C_D)/d(C_{L_N}-C_{L_{\min}})^2$
dC_m/dC_L	= pitching-moment curve slope at $\alpha=0$
L/D	= ratio of lift to drag
M	= Mach number
q	= freestream dynamic pressure
S	= wing area, 1365.1 cm^2 (211.59 in.^{2})
t	= profile thickness
y	= spanwise distance from vertical plane of symmetry of the body
z	= vertical distance above wing chord plane
α	= angle of attack
Λ	= sweep angle measured between a perpendicular to the body axis and the 0.25c line of the wing in a horizontal plane (for the oblique wing, the right wing tip is forward for $+\Lambda$)

Subscripts

L.E.	= leading edge
max	= maximum
min	= at minimum drag
N	= at given value N
SF	= skin friction
vort	= vortex

Introduction

USING an oblique wing configuration to reduce wave drag at transonic and supersonic Mach numbers is not new.[1-5] Recent experimental measurements[6,7] have been made for such a configuration designed with relatively high aspect-ratio wing of 12.7 (based on the unswept span) which is expected to have application to a transonic/supersonic transport airplane. The present investigation explored the aerodynamic efficiency of a low aspect-ratio oblique wing mounted on a top of a body of revolution, which might have application to a fighter-type vehicle. To compare aerodynamic efficiency, some results are presented for oblique and swept wings having 45° of sweepback and an aspect ratio of 3.7 (the same as the oblique wing when swept 38°). The basic data from this study have been presented without theoretical analysis,[8] whereas the main emphasis in the present paper is on comparing the experimental results at low angles of attack with the results from linear theory.

Since the spanwise distribution of lift due to angle of attack on oblique wings is asymmetric, asymmetric tip stalling is likely on flat oblique wings, resulting in nonlinear aerodynamic moment curves. To alleviate this problem, two different spanwise bends or washouts were investigated on the oblique wing; hereinafter, these bends are referred to as "small" or "large." To study the effect of wing bend on experimental forces and moments, oblique wings having these two bends are compared with each other and with the swept wing at Mach numbers of 0.6 and 0.95.

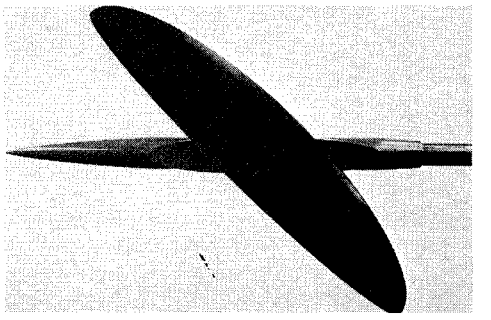

Fig. 1 Oblique wing-body combination ($\Lambda=45°$).

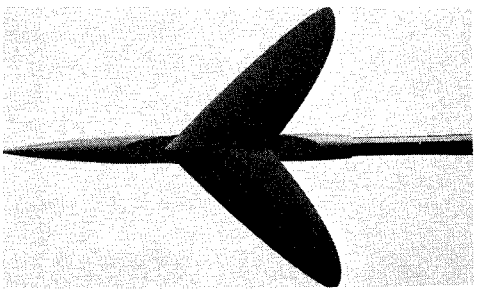

Fig. 2 Swept wing-body combination.

Presented as Paper 74-771 at the AIAA Mechanics and Control of Flight Conference, Anaheim, California, August 5-9, 1974; submitted August 9, 1974; revision received January 13, 1975.

Index categories: Aircraft Configuration Design; Aircraft Aerodynamics (including Component Aerodynamics); Aircraft Performance.

*Research Scientist. Associate Fellow AIAA.
†Research Scientist.

Test Facilities and Model Description

Tests were conducted in the Ames 6- by 6-Foot Wind Tunnel, which is a variable pressure, continous flow, closed return type facility. The Mach number can be varied during continuous operation from 0.6 to 2.2 by moving an asymmetric nozzle block. For transonic testing, the boundary layer was removed through the perforated ceiling and floor.

The model was an oblique or fixed, swept wing, mounted separately on a Sears-Haack body of revolution (designed to have minimum wave drag for a given length and volume). The oblique wing was elliptical in planform, as shown in Fig. 1, and had an aspect ratio of 6.0 based on the unswept span. This wing was tested with sweep angles of 0, 45°, 50°, 55°, and 60°. The fixed swept wing ($\Lambda = 45°$) also had an elliptical planform, as shown in Fig. 2, and an aspect ratio of 3.7 (for comparison, the oblique wing has an aspect ratio of 3.7 at a sweep angle of 38°). Each wing had a Garabedian profile (designed for $C_L = 1.3$ at $M = 0.6$ with $(t/c)_{max} = 0.1016$) perperpendicular to the 0.25 chord line and an elliptical spanwise variation of $(t/c)_{max}$ from 0.11 at the wing root to 0.06 at the wing tip. Complete geometrical details of both wings, their profiles and the body of revolution are given in Ref. 8 (Tables 1-3 and Fig. 2).

Figure 3 shows spanwise upward wing bends or washouts that were investigated on the oblique wing. As the wing was bent upward, the wing chords perpendicular to the 0.25c line were kept parallel to a horizontal plane. The swept wing had the same bend distribution as the small bend for the oblique wing. Upward bending of both wing panels on the oblique wing results in washout on the downstream panel and washin on the upstream panel, whereas upward bending on the swept wing results in washout on both panels.

Data Reduction and Test Condition

The models were sting-supported through the base of the body on a 6-component strain-gage balance as indicated in Fig. 1. Measured axial forces were corrected to a condition corresponding to having the freestream static pressure on the base of the model. Moment centers for the oblique and swept wing models were at different longitudinal stations, as shown in Ref. 8 (Figs. 2c and 2d). For the oblique wing, the moment center was at $0.40c_{root}$ ($\Lambda = 0$); for the swept wing, the moment center was at $0.25\bar{c}$, where $\bar{c} = \int c^2 dy / \int c dy$. The same reference lengths and areas were chosen for the oblique and swept wings, namely, $\bar{c} = 20.88$ cm, $b = 71.12$ cm, and $S = 1365.1$ cm^2.

The boundary layer was tripped 0.762 cm downstream of the leading edge and 2.54 cm downstream of the body nose by 0.0191-cm glass spheres, as substantiated by sublimation studies. The effect of sphere drag on total wing-body drag was too small to require correction.

The unit Reynolds number was held constant at 8.2×10^6/m except for the unswept, oblique wing with small bend, for which the unit Reynolds number was reduced to 5.58×10^6/m because of dynamic overload restrictions for the balance. The angle-of-attack range was from $-3°$ to 31°, and the Mach number range was from 0.6 to 1.4. The angle of attack was indicated by an electrical dangleometer mounted in the sting, corrections being applied for balance and sting deflections.

Theoretical Methods

Linear theory based on a matrix-panel method was used for the lift, drag, and pitching-moment predictions. In this method the wing and body are represented by a large number of panels (100 for the wing and 80 for the body). Singularities in the plane of the wing, on the surface of the body, and along the body axis were used to define the matrix of aerodynamic influence coefficients that satisfied the boundary condition of zero velocity component perpendicular to each panel at a specified control point. For subsonic Mach numbers, the control points on each panel were downstream 85% of the panel chord; for supersonic Mach numbers, they were downstream 95% of the panel chord to provide stable solutions. This method includes effects from wing thickness and camber, from body thickness and camber, and from the mutual interference of the wing and the body. The original program was developed by Woodward et al.[9] In the present paper, lift, aerodynamic-center location, and span loading were calculated from the matrix-panel method, but drag was calculated by two different procedures designated "no leading-edge thrust" and "full leading-edge thrust." At Mach numbers having no assumed leading-edge thrust, the induced drag due to lift (including the wave drag at supersonic Mach numbers) was calculated from the near field, the resultant force on each panel being perpendicular to the panel surface. At all Mach numbers with full leading-edge thrust assumed, the vortex drag due to lift was calculated from the span loading, following the Max Munk stagger theorem.[10] At supersonic Mach numbers with full leading-edge thrust assumed, the wave drag due to lift was calculated by collapsing the wing-body combination into an equivalent body of revolution.[11] This wave drag, which varied with lift, was added to the vortex drag due to lift to obtain the total drag due to lift. For all cases, skin-friction drag, which was assumed constant with lift, was calculated from the reference-temperature method of Sommer and Short.[12] Finally, the important aerodynamic parameters were calculated from an assumed parabolic drag polar for a cambered wing ($C_{D_{min}}$ occurs at a positive C_L) as sketched in Fig. 4. From the definitions of the coefficients in Fig. 4, the total drag at a given lift is

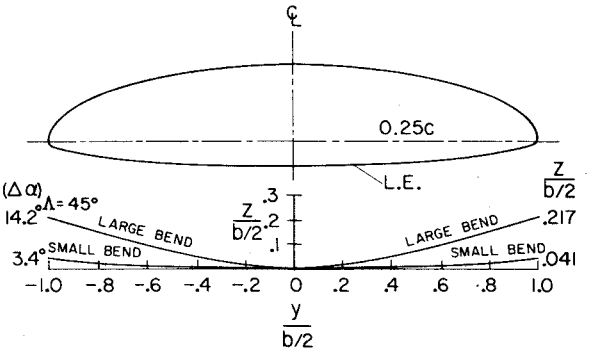

Fig. 3 Wing bends.

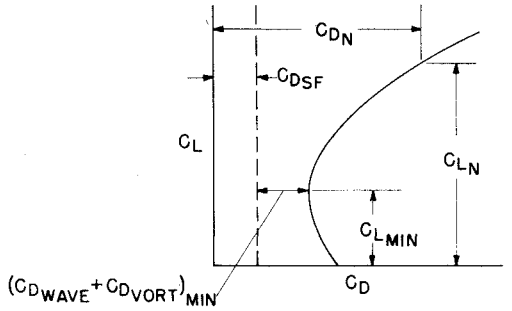

Fig. 4 Drag polar.

$$C_{D_N} = C_{D_{SF}} + (C_{D_{wave}} + C_{D_{vort}})_{min} + K(C_{L_N} - C_{L_{min}})^2 \quad (1)$$

From three sets of C_{D_N} and C_{L_N}, Eq. (1) will give three simultaneous equations from which the following quantities can be derived:

$$C_{L_{min}} = \frac{(C_{D_3} - C_{D_1})C_{L_2}^2 + (C_{D_2} - C_{D_3})C_{L_1}^2 + (C_{D_1} - C_{D_2})C_{L_3}^2}{2[(C_{D_3} - C_{D_1})C_{L_2} + (C_{D_2} - C_{D_3})C_{L_1} + (C_{D_1} - C_{D_2})C_{L_3}]} \quad (2)$$

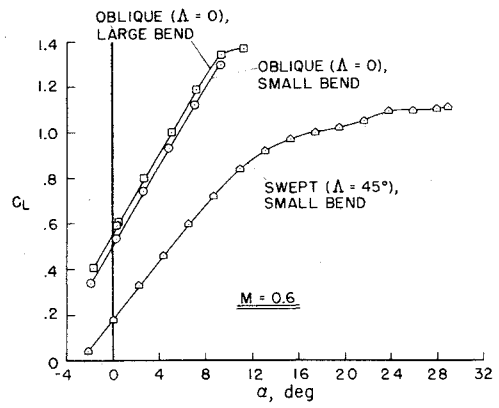

Fig. 5 Experimental lift.

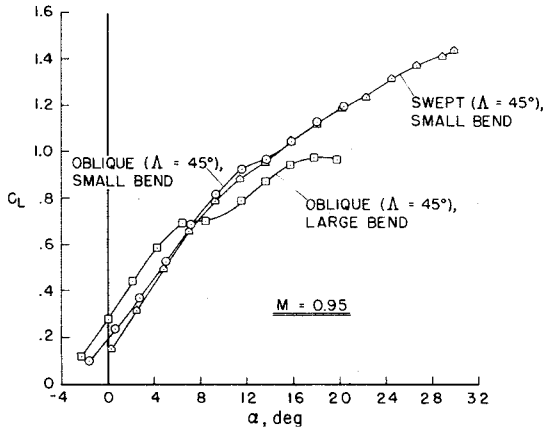

Fig. 6 Experimental lift.

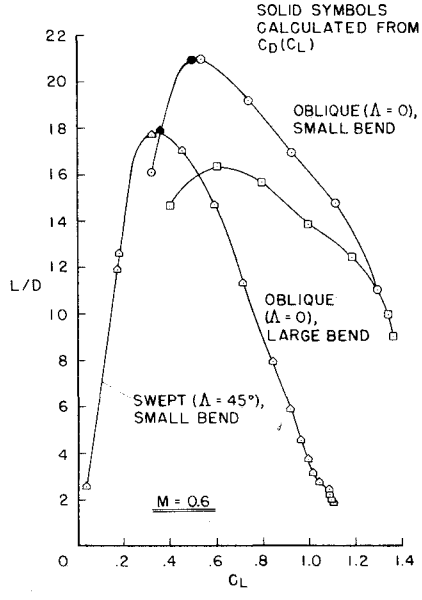

Fig. 7 Experimental lift-to-drag-ratio.

$$K = \frac{C_{D_1} - C_{D_2}}{(C_{L_1} - C_{L_{\min}})^2 - (C_{L_2} - C_{L_{\min}})^2} \tag{3}$$

$$C_{D_{\min}} = C_{D_N} - K(C_{L_N} - C_{L_{\min}})^2 \tag{4}$$

$$C_{D_N} = (C_{D_{SF}} + C_{D_{wave}} + C_{D_{vort}})_N \tag{5}$$

$$(L/D)_{\max} = \frac{1}{2K\left[\left[(C_{D_{\min}}/K) + C_{L_{\min}}^2\right]^{1/2} - C_{L_{\min}}\right]} \tag{6}$$

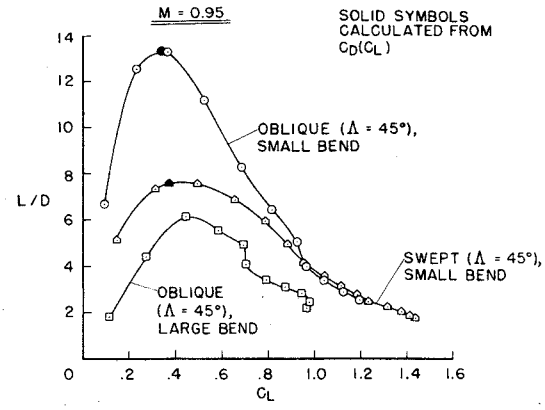

Fig. 8 Experimental lift-to-drag ratio.

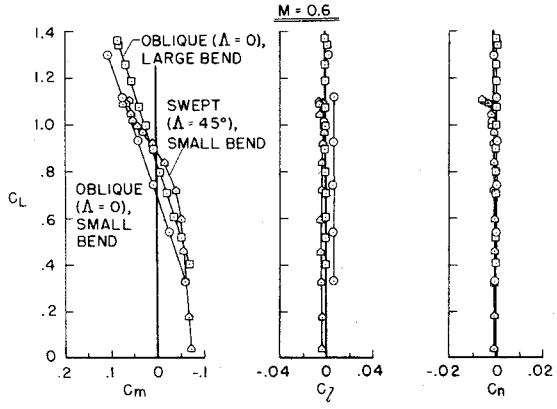

Fig. 9 Experimental pitching, rolling, and yawing moments.

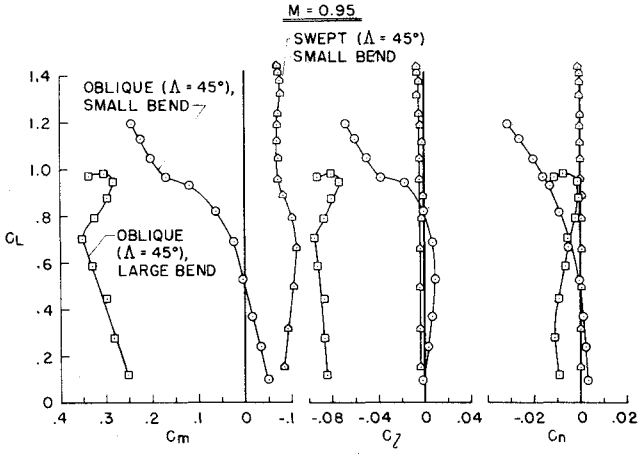

Fig. 10 Experimental pitching, rolling, and yawing moments.

$$(C_L)_{(L/D)_{\max}} = \left[\frac{C_{D_{\min}}}{k} + C_{L_{\min}}^2\right]^{1/2} \tag{7}$$

The experimental drag polar was ill-defined at low lift because of insufficient data. Consequently, for each configuration, three sets of experimental lift and drag were used in Eqs. (2-4, 6 and 7) to obtain the desired parameters.

Results and Discussions

Figures 5-10 compare an oblique wing with large and small bends to a swept wing with small bend for Mach numbers of 0.6 and 0.95. Figures 11-16 compare summary experimental parameters for both the oblique and swept wings with small bend to theoretical values throughout the Mach number range of 0.6-1.4.

As expected, at Mach number 0.6 (Fig. 5), the unswept oblique wing ($\Lambda = 0$ is optimum at $M = 0.6$) with either bend

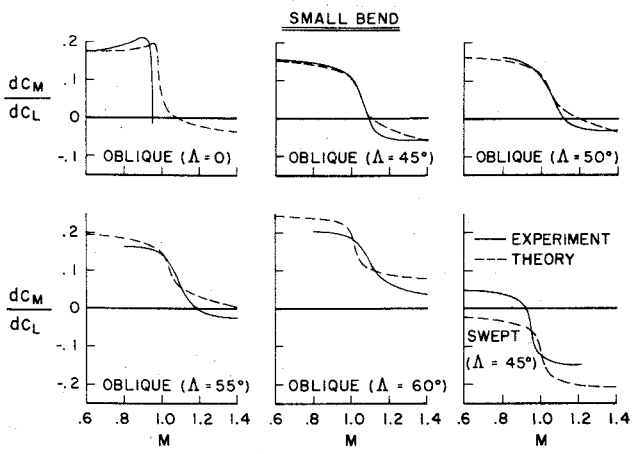

Fig. 11 Experimental and theoretical pitching-moment curve slopes.

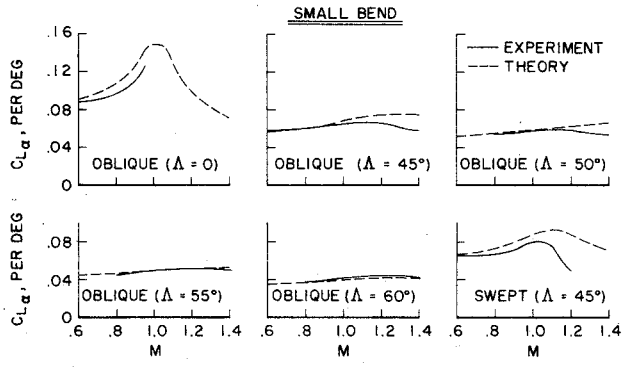

Fig. 12 Experimental and theoretical lift-curve slopes.

had more lift for a given angle of attack than the fixed swept wing because the unswept oblique wing has (a) a higher aspect ratio and (b) lesser sweep than the swept wing. At Mach number 0.95 (Fig. 6), the oblique ($\Lambda = 45°$) and swept wings (both with small bend) have nearly the same lift at angles of attack above 4°; however, the oblique wing (with large bend) exhibited a large change in the lift-curve slope near $\alpha \simeq 6°$, a result associated with flow separation from the upstream wing tip (substantiated by tuft studies[8]). At Mach number 0.6 and at the higher C_L's (Fig. 7), both oblique wings ($\Lambda = 0$) exhibt higher L/D ratios than the swept wing as would be expected from aspect ratio and sweep considerations. The oblique wing with small bend having higher L/D ratios than the oblique wing with large bend may be related to Reynolds number differences, 5.58×10^6/m and 8.2×10^6/m being used for the small and large bends, respectively. Note that the solid points for $(L/D)_{max}$ interpolated from the $C_D(C_L)$ experimental data as described before agree quite well with the faired $L/D(C_L)$ curves. At Mach number 0.95 (Fig. 8), the oblique wing ($\Lambda = 45°$) with small bend has considerably larger L/D's than the swept wing, especially for the important cruise C_L's up to about 0.9. Again, the increase in drag associated with flow separation was so severe at this Mach number for the oblique wing ($\Lambda = 45°$) with large bend that lower L/D's were measured at all C_L's for this wing than for the swept wing. This emphasizes the large drag penalty induced by flow separation from selecting too large an upward bend of the oblique wing panel. At Mach number 0.6 (Fig. 9), the oblique wing ($\Lambda = 0$) has the expected linear pitching-, rolling-, and yawing-moment curves; however, the swept wing would exhibit the usual pitch-up tendency typical of this type of wing at C_L's above 0.7, if a reasonable center-of-gravity location were selected to give positive longitudinal stability at low C_L's. At Mach number 0.95 (Fig. 10), the oblique wing ($\Lambda = 45°$) has nonlinear pitching-, rolling-, and yawing-moment curves, which indicate the strong influence of wing bend on the linearity of the moment curves. For example, the oblique wing with large bend would have a pitch-down tendency above $C_L = 0.7$, but the oblique wing with small bend would have a pitch-up tendency—both results known to be related to whether the forward or rearward wing panel stalls first. It is reasonable to expect, therefore, that an intermediate bend on the oblique wing could produce nearly linear curves. In Fig. 10 the swept wing again exhibits a pitch-up tendency near $C_L = 0.7$.

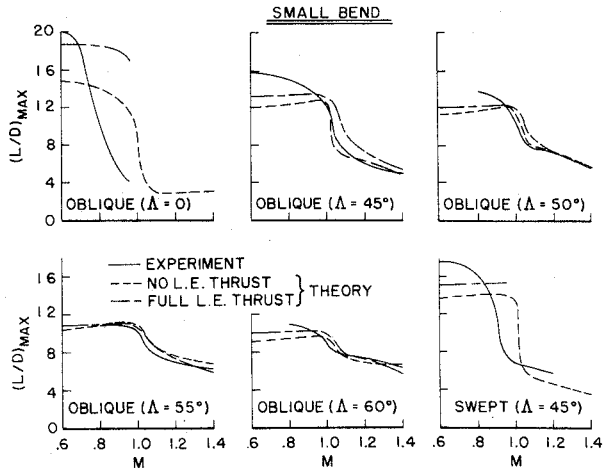

Fig. 13 Experimental and theoretical maximum lift-to-drag ratios.

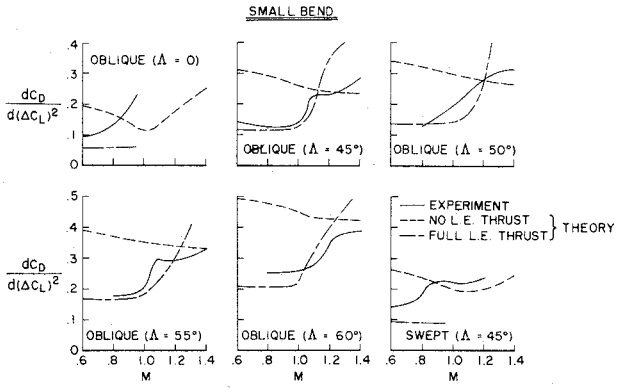

Fig. 14 Experimental and theoretical drag due to lift factors.

Pitching-moment curve slopes (Fig. 11) indicate that the aerodynamic center was predicted and measured to move rearward about $0.20\bar{c}$ with Mach number for the oblique wing at sweep angle and for the swept wing; however, the absolute level of dC_m/dC_L for the swept wing was not correctly predicted.

Lift-curve slopes (Fig. 12) for both wings at subsonic Mach numbers were predicted within 10%, but at supersonic Mach numbers the oblique wing at $\Lambda = 45°$ and 50° and the swept wing had considerably lower C_L than predicted. At $M = 0.6$ (the design Mach number for the Garabedian profile), the predicted values of $(L/D)_{max}$ for the unswept oblique wing with full leading-edge thrust (Fig. 13) agree better with experiment than values with no leading-edge thrust. With the oblique wing at $\Lambda = 0$ for $M \tilde{>} 0.7$, the predicted values of $(L/D)_{max}$ were considerably above the experimental values, because of the high experimental drag caused by shockwave-induced flow separation. Predicted values of $(L/D)_{max}$ for the oblique wing at other sweep angles generally agreed with the measured values at supersonic Mach numbers, independent of leading-edge thrust assumption. At low subsonic Mach numbers, however, the assumption of full leading-edge thrust improved the agreement slightly for both wings. In general, predicted values of $dC_D/d\Delta C_L^2$, and $C_{D_{min}}$, and $(C_L)_{(L/D)_{max}}$ for the oblique wing (Figs. 14 and 16) show better agreement with experiment at low subsonic Mach numbers with full leading-edge thrust assumed, but at supersonic Mach numbers the proper choice of leading-edge thrust assumption

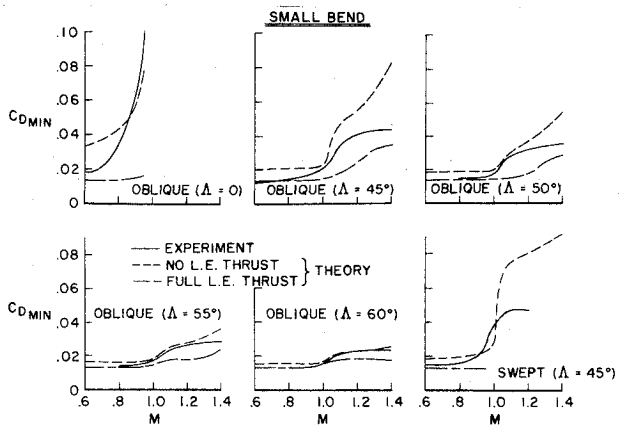

Fig. 15 Experimental and theoretical minimum drag.

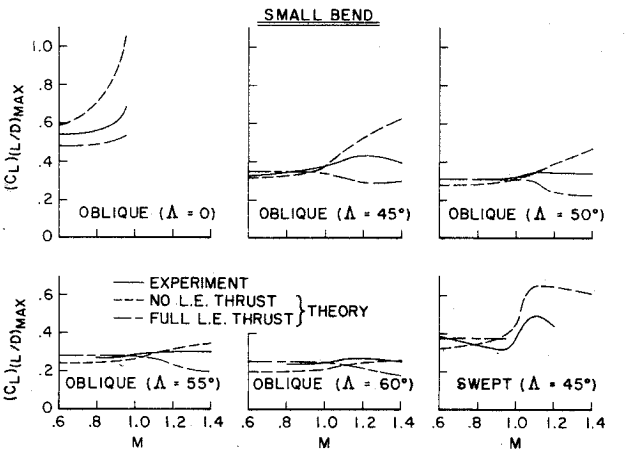

Fig. 16 Experimental and theoretical lift at maximum lift-to-drag ratio.

is unclear. The agreement between theory and experiment was generally better for $(L/D)_{max}$ and nearly independent of the leading-edge thrust assumption than was found generally for the factors from which $(L/D)_{max}$ was calculated. This effect is illustrated by a typical drag polar (Fig. 17) where a distinct improvement in the agreement is shown between the theoretical and experimental polars by assuming full leading-edge thrust, but no difference for $(L/D)_{max}$ for either leading-edge thrust assumption.

With the oblique wing set near its optimum sweep angle for a given Mach number (Fig. 18), the oblique wing shows higher values of $(L/D)_{max}$ than for the fixed, swept wing at all Mach numbers. If this comparison had been made between an oblique and a conventional variable swept wing rather than a fixed swept wing, the same improvement for the oblique wing would have been realized at a Mach number of about 0.95, since about 45° of sweep is required. At Mach numbers below and above 0.95, however, the difference would have been smaller but still favorable for the oblique wing.

Conclusions

Maximum lift-to-drag ratio was larger at all Mach numbers for the oblique wing set at its optimum sweep angle for a given Mach number than for the fixed, swept wing. Results from the oblique wing with two different spanwise upward bends indicate that an intermediate bend distribution would produce more linear pitching-, rolling-, and yawing-moment curves. Linear theory generally gave good estimates of the aerodynamic-center travel with Mach number, the subsonic lift-curve slopes, and the maximum lift-to-drag ratios (independent of the assumption on leading-edge thrust); however, the minimum drag, and the drag due to lift at subsonic Mach numbers were generally predicted better with full leading-edge thrust assumed.

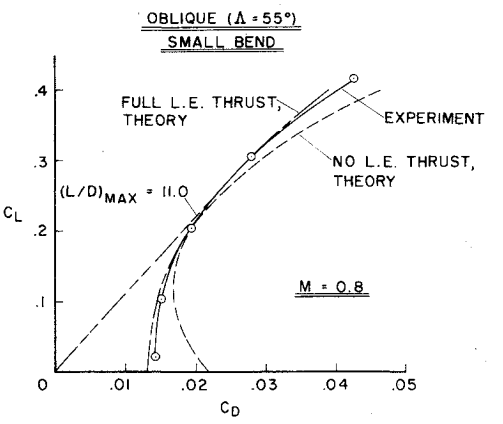

Fig. 17 Experimental and theoretical drag polars.

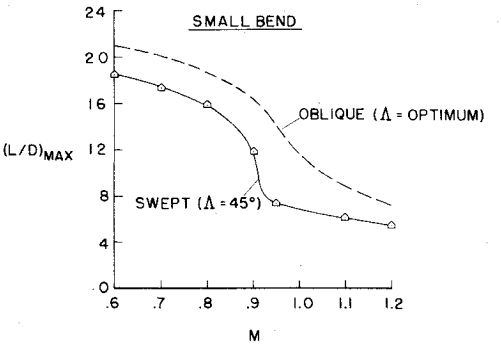

Fig. 18 Experimental maximum lift-to-drag ratios.

References

[1] Jones, R. T., "Theoretical Determination of the Minimum Drag of Airfoils at Supersonic Speeds," *Journal of Aeronautical Sciences*, Vol. 19, Dec. 1952, pp. 813-822.

[2] Jones, R. T., "Reduction of Wave Drag by Antisymmetric Arrangement of Wings and Bodies," *AIAA Journal*, Vol. 10, Feb. 1972, pp. 171-176.

[3] Lee, G. H., "Slewed Wing Supersonics," *The Airplane*, Vol. 100, March 1961, pp. 240-241.

[4] Smith, J. H.B., "Lift/Drag Ratios of Optimized Slewed Elliptic Wings at Supersonic Speeds," *The Aeronautical Quarterly*, Royal Aeronautical Society, Vol. XII, Aug. 1961, pp. 201-218.

[5] Jones, R. T., "New Goals and a New Shape for the SST," *Astronautics and Aeronautics*, Vol. 10, Dec. 1972, pp. 66-70.

[6] Graham, L. A., Jones, R. T., and Boltz, F. W., "An Experimental Investigation of an Oblique-Wing and Body Combination at Mach Numbers Between 0.60 and 1.40," TM X-62,207, Dec. 1972, NASA.

[7] Graham, L. A., Jones, R. T., and Boltz, F. W., "An Experimental Investigation of Three Oblique-Wing and Body Combinations at Mach Numbers Between 0.60 and 1.40," TM-X-62,256, April 1973, NASA.

[8] Hopkins, E. J., Meriwether, F. D., and Pena, D. F., "Experimental Aerodynamic Characteristics of Low-Aspect Ratio Swept and Oblique Wings at Mach Numbers Between 0.6 and 1.4," TM X-62,317, Nov. 1973, NASA.

[9] Woodward, F. A., Tinoco, E. N., and Larsen, J. W., "Analysis and Design of Supersonic Wing-Body Combinations, Including Flow Properties in the Near Field, Part I—Theory and Application," CR-73,106, Aug. 1967, NASA.

[10] DeYoung, J. and Harper, C. W., "Theoretical Symmetric Span Loading at Subsonic Speeds for Wings Having Arbitrary Plan Form," Tech. Rept. 921, 1948, NASA.

[11] Harris, Jr., R. V., "A Numerical Technique for Analysis of Wave Drag at Lifting Conditions," TN D-3586, Oct. 1966, NASA.

[12] Sommer, S. C. and Short, B. J., "Free-Flight Measurements of Turbulent-Boundary-Layer Skin Friction in the Presence of Severe Aerodynamic Heating at Mach Numbers from 2.8 to 7.0," TN 3391, 1955, NACA. (Also, *Journal of Aeronautical Sciences*, Vol. 23, June 1956. pp. 536-542.)